Self noise produced by an airfoil with non-flat plate trailing edge serrations

Tze Pei. Chong[1] and Alexandros Vathylakis[2]
School of Engineering and Design, Brunel University, Uxbridge, UB8 3PH, United Kingdom

Phillip F. Joseph[3]
ISVR, University of Southampton, Southampton, SO17 1BJ, United Kingdom

and

Mathieu Gruber[4]
Snecma Villaroche, Acoustic Department, 77550 Moissy Cramayel, France

This paper represents the results of an experimental study aimed at reducing the airfoil self-noise by the trailing edge serration of four different sawtooth geometries (defined in the serration angle and length). These serrations have a common feature: all of the sawtooth patterns are cut directly into the trailing edge of a realistic airfoil. This configuration offers better structural strength and integrity. For the sawtooth trailing edges investigated here, the radiation of the extraneous vortex shedding noise in a narrowband frequency due to the partial bluntness at the serration roots is unavoidable. However, this narrowband component tends to be less significant provided that the serration angle is large and the serration length is moderate. Sound power was measured, and some of the sawtooth geometries have been shown to afford significant boundary-layer instability tonal noise and moderate turbulent broadband noise reductions across a fairly large velocity range. This paper demonstrates that a nonflat plate serrated trailing edge can also be effective in the self-noise reduction. Some experimental results are also presented in order to explain the self-noise mechanisms.

[1] (corresponding author). Lecturer, School of Engineering and Design, t.p.chong@brunel.ac.uk, AIAA Member.
[2] PhD student, School of Engineering and Design, alexandros.vathylakis@brunel.ac.uk, Non AIAA member.
[3] Professor, Institute of Sound and Vibration Research, pfj@isvr.soton.ac.uk, AIAA Member.
[4] Engineer, SNECMA, mathieu.gruber@snecma.fr, AIAA Member.

Nomenclature

$2h$ = *serration length (root-to-tip distance), mm*

e_i, e_j = *raw signals from the surface mounted thin films, V*

c_o = *speed of sound, ms^{-1}*

C = *airfoil chord length, m*

f = *frequency, Hz*

f_d = *tonal frequency due to bluntness produced by the serrated trailing edge airfoil, Hz*

L = *acoustic radiation term*

I_y = *spanwise correlation length, mm*

r = *distance between the airfoil trailing edge to the microphone, m*

S_{pp} = *noise spectrum, dB*

S_{qq} = *wall pressure spectrum, dB*

U = *mean flow velocity, ms^{-1}*

v_i, v_j = *streamwise turbulence velocities in the airfoil wake, ms^{-1}*

W = *sound power level, W*

W_{ref} = *reference sound power level, 10^{-12} W*

x = *streamwise direction measuring from the airfoil leading edge, mm*

y = *wall-normal direction, mm*

Δt = *time difference between each frames in Fig. 13, s*

δ = *boundary layer thickness, mm*

ε = *bluntness of the saw tooth trailing edge at the root region, mm*

Φ = *cross-spectrum or auto-spectrum of the streamwise velocities or thin film signals, $(ms^{-1})^2$/Hz or $(V)^2$/Hz*

γ^2 = *coherence of the streamwise velocities in the airfoil wake; coherence of the signals of the thin film array*

φ = *serration angle, deg*

λ = *serration period, mm*

Θ = *polar angles of the microphone relative to the jet flow centerline, deg*

θ = *angle of attack for the airfoil, deg*

ρ = *air density, kgm^{-3}*

I. Introduction

Recently, there has been much interest in developing control methods aimed at reducing trailing-edge self-noise. Approaches taken include serrated edges [1–3], a porous surface [4], and brushes [5,6]. These passive methods have been demonstrated experimentally in low-speed rig tests to afford reductions in noise radiation between 3 and 7 dB. One of the most promising treatments has been the use of serrated trailing edges. In nearly all cases, however, the serrations have been cut into flat plates and then inserted into the trailing edge of the main airfoil body. This has been primarily to avoid the vortex shedding noise that arises due to the introduction of bluntness caused by cutting serrations into the airfoil body. The obvious disadvantage of using flat plate inserts is that it clearly does not have the strength and integrity required for their intended applications of wind turbines, propellers, and rotor blades. The addition of flat plate inserts in airfoils could also potentially result in deteriorations in their aerodynamic performance. For a highly cambered airfoil, the level of the adverse pressure gradient present at the flat plate insert at the suction surface could be high enough to trigger turbulent separation and produce additional noise sources. Therefore, at a particular combination of airfoil geometry, Reynolds number and angle of attack, it is possible that the amount of noise reduction by the flat plate serrations is partially masked by additional noise sources. This may be one of the reasons why there is such a large discrepancy between the measured and predicted noise reductions [1,7].

Figure 1 defines the serration period λ, the serration angle φ, and the serration length (root-to-tip distance) $2h$ associated with a sawtooth serration. For the case of nonflat plate serrated trailing edge, an extra parameter of the root bluntness ε is also introduced.

At a low Reynolds number and with low-freestream turbulence intensity, the lack of bypass transition mechanisms on the airfoil surfaces can promote the appearance of Tollmien–Schlichting (T–S) instability waves. On a conventional sharp-edged airfoil, the presence of a locally adverse pressure gradient near the trailing edge can amplify these instability waves, leading to the radiation of self excited high-amplitude tones [8–13]. Lowson et al. [8] observed that T–S waves by themselves may not be the only mechanism that generates noise. They stated that the generation of laminar instability noise must be accompanied by the presence of a separation bubble, which acts as an amplifier for the most unstable T–S modes near the trailing edge. Support for this observation is provided in more recent works [9–12], although definitive proof that a separation bubble is needed for the appearance of T–S tones is not yet available.

Assuming the correctness of this hypothesis, an effective strategy for reducing airfoil tonal noise due to T–S waves is to inhibit the separation region near the trailing edge, which can be achieved by either active or passive flow control approaches. As will be shown later in the paper, when a trailing-edge serration is introduced, an otherwise laminar or separated boundary layer near a nominally sharp trailing edge can force the bypass transition to turbulence. This has the effect of suppressing boundary-layer instability tonal noise. The effect of serration parameters, such as λ, φ, and $2h$, on the level of airfoil boundary-layer instability tonal noise reduction for laminar boundary layers will be investigated in this paper.

In the case of a fully turbulent boundary layer, for example at a high Reynolds number, or when tripping is applied, some of the turbulent energy in the boundary layer will be scattered into broadband noise at the trailing

edge. Typical broadband noise amplitudes are considerably lower than the boundary-layer instability tonal noise discussed previously. The relationship between the far-field acoustical pressure and the near-field surface pressure near the trailing edge is made explicit in [14], which derived a direct relationship between the power spectral density (PSD) of the far-field noise S_{pp} in terms of the spanwise correlation length I_y and the surface pressure spectrum S_{qq} near the trailing edge, and a radiation term $L(\omega)$, of the form

$$S_{pp}(\omega) \propto L(\omega) I_y(\omega) S_{qq}(\omega) \,, \tag{1}$$

This result predicts a reduction in the radiated broadband noise if the level of either I_y, S_{qq}, and/or $L(\omega)$ is reduced. Because a sawtooth trailing edge will be shown later to trigger an otherwise laminar boundary layer into a turbulent one (see in Sec. III.A), it is not expected to change the level of S_{qq} significantly compared to the sharp-edge baseline case. This conjecture is consistent with the findings in [15] from a Direct Numerical Simulation study of serrated trailing-edge noise.

The relationship between the serration parameters, such as λ, φ, and $2h$, and the radiated broadband noise has been studied theoretically by Howe [7], whereby the greatest noise reductions are predicted in the high-frequency range $\omega h / U \gg 1$ and for $\varphi < 45$ deg, for which noise reductions of about $10 \log_{10} [1 + (4h/\lambda)^2]$ dB are predicted. This implies that an 18 dB broadband noise reduction can theoretically be achieved by one of the serration configurations investigated in the current study for which $h / \lambda \approx 2$ (S1, see Table 1). However, subsequent experimental work by Gruber et al. [1] has shown that although the best reductions are obtained for the smallest φ value, these noise reductions are limited to the low frequency range of $\omega\delta / U < 1$, which is in direct contradiction with Howe's predictions, where δ is the boundary-layer thickness. Moreover, Gruber et al. [1] has also found that the serration length ($2h$) must be greater than the trailing-edge boundary-layer thickness (i.e., $h / \delta > 0.5$) for significant noise reductions to occur. For all the 36 different sawtooth flat plate inserts that were tested by Gruber et al. [1], maximum noise reductions were limited to 7 dB. Gruber et al. [1] also observed noise increases of up to 3 dB at high frequencies, which they attributed to the presence of small jets through the troughs of the serration.

In this paper, we investigate the noise performance of serrations cut directly into the main body of a realistic airfoil, thus preserving its original overall shape. We will present experimental results to show that the boundary-layer instability tonal noise radiation can be inhibited significantly by this type of serration. We further show that when the boundary layer becomes turbulent, moderate broadband noise reductions can be obtained, which are similar to that of flat plate inserts but at the expense of generating narrowband noise due to the vortex shedding that is caused by the partial bluntness introduced at the root of the serration. One of the main objectives of this paper is to present a strategy of reducing the impact of this extraneous noise by careful choice of the serration geometry.

Section II describes details of the test model, experimental setup, instrumentation, and experimental technique. Section III presents boundary-layer measurements made on the surface of the sawtooth. This section also contains the results of the boundary layer with and without artificial tripping on the airfoil surfaces and the determination of boundary-layer separation on the pressure surface of an airfoil. Noise measurements are mainly presented in Sec. IV, which is broken down into two subsections. Section IV.A presents the reductions in tonal noise that occurs at a low Reynolds number due to hydrodynamic instabilities in the laminar boundary layer, which from hereon will be referred to as "instability tonal noise." Section IV.B concerns the reductions in broadband noise for the case of a full

turbulent boundary layer. Section V contains a general discussion on the noise results. Conclusions and a suggested future work are included in Sec. VI.

II. Experimental Setup

A. Test Model and the Trailing-Edge Serrations

The airfoil under investigation in this paper is aNACA0012 airfoil with a 0.15 m chord (C) and 0.45 m span. From $x/C = 0$ (leading edge) to $x/C = 0.79$ is the originalNACA0012 airfoil body, where x is the streamwise direction. Further downstream, $0.79 < x/C < 1.0$, is a section that can be removed and various serration geometries can be attached. Once attached, the serrations form a continuous profile, giving the appearance that the serrations are cut into the main body of theNACA0012 airfoil as shown in Fig. 1. A total of five trailing-edge sections, including one with a sharp trailing edge to serve as the baseline case, were used.

Miniatures microphones of the Knowles WP-3502 type were embedded inside the airfoil's main body. Each of these microphones is used to measure the wall pressure fluctuations via sensing holes of 0.5 mm in diameter on both of the lower and upper surfaces of the midspan plane along the airfoil chord. There are 15 microphones on each surface that cover $0.09 < x/C < 0.64$. In the current study, only the unsteady wall pressure results obtained at $x/C = 0.64$ were shown in order to represent the states of the boundary layers at the airfoil's aft region.

In this study, four nonflat plate-type serrated trailing edges were tested for their effectiveness in the reductions of both boundary-layer instability tonal noise and turbulent boundary-layer broadband noise. Table 1 summarizes the geometrical parameters of these serrations in terms of φ, $2h$, λ/h, and ε (ε is the bluntness at the root). Note that S0 represents the baseline sharp trailing edge. Serrations S1–S3 have the same $2h$ and ε but different φ and λ/h. Serrations S2 and S2* have the same φ and λ/h but different $2h$ and ε.

B. Wind Tunnel Facilities and the Instrumentations

Free-field measurements of the airfoil self-noise were conducted in the open jet wind tunnel in the Institute of Sound and Vibration Research (ISVR) at the University of Southampton, which is situated in an 8 × 8 ×8 m anechoic chamber. The nozzle exit is a rectangular section with a dimension of 0.15 (height) × 0.45 m (width). This wind tunnel can achieve turbulence intensity as low as 0.1% and a Mach number as high as 0.3 while maintaining a low background noise [16].

The range of jet speeds under investigation was between 20 ms^{-1} and 60 ms^{-1}, corresponding to Reynolds numbers based on C of 2×10^5 and 6×10^5, respectively. The airfoil was held by side plates and attached to the nozzle lips. In this study, the self-noise of the airfoil at a 15 deg geometrical angle of attack was investigated corresponding to an effective angle of attack, $\theta = 4.2$ deg, once the downwash deflection of the incident flow by the airfoil is taken into account using the two-dimensional open wind-tunnel correction scheme in [17]. At this angle of attack, any possible confinement effect that might be caused by the nozzle geometry should be investigated. For this purpose, a hot wire was used to measure the airfoil wake profile at a position 5mmbehind the trailing edge at a jet

speed of $U = 30$ ms^{-1}. A color map of the velocity PSD versus flow speed is plotted in Fig. 2. From the figure, it is clear that the nozzle shear layers (which are characterized by a high amplitude with broadband frequencies in the PSD), as well as the low-turbulence free jet, were both deflected by the presence of the airfoil. The measured airfoil wake is shown to be well clear of the nozzle shear layers. Therefore, the shear layers impingement on the trailing edge, which would have significant impact on the radiated noise, is not expected to occur in the current study.

As shown in Fig. 3, far-field noise measurements were made by seven microphones uniformly distributed between the polar angles from $\Theta = 50$ to 110 deg at a distance of 1.25 m from the airfoil trailing edge at midspan. Note that the noise measurements at $\Theta < 50$ and $\Theta > 110$ deg were not attempted due to the potential acoustic interference from the jet noise and the acoustic reflection of the solid wind-tunnel wall, respectively. Noise data were sampled at 30 kHz for 13.33 s by a 24 bit analog-digital card from National Instruments. In addition to an analog low-pass antialias filter, the data were further filtered at more than one-half of the sampling frequency to minimize further the effects of aliasing. The data were then windowed (with a size of 4096 points) and averaged to obtain the power spectra density of the noise with a resolution of a 1 Hz bandwidth.

Unless otherwise stated, a single hot-wire probe (5 μm in diameter and a 1.25 mm length, DANTEC 55P11) was used to measure the mean and fluctuating velocities at an overheat ratio of 1.8. Signals from the hot wire were digitized by a 12 bit analog-to-digital (A/D) converter (TSI model ADCPCI) at a sampling frequency of 5 kHz for 32,768 realizations. In this case, only an analog low-pass filter was employed, and the data were filtered at 2.5 kHz.

Thin surface-mounted hot-film arrays were employed in the present study to identify the separation point near the untripped airfoil's pressure surface trailing edge. The DANTEC 55R47 type glue-on thin film has an overall thickness of 50 μm. The sensing element is 0.9 × 0.1 mm and is connected to gold-plated leads. An overheat ratio of 1.3 was employed for these thin films to establish reasonable velocity sensitivity and minimal thermal destabilization to the boundary layer. The arrangement of the thin-film array is shown in Fig. 4. Each thin film is labeled as HF1, HF2, and so on. The sensing elements of HF1, HF2, HF3, HF4, and HF5 are located at $x/C = 0.79$, 0.83, 0.87, 0.91, and 0.95, respectively. Each thin film has an 8 mm spanwise offset to each other in order to avoid flow interference. This arrangement is appropriate for the current study due to the predominantly two-dimensional nature of the laminar separation and the T–S instability waves. The signals from the thin films were sampled simultaneously at 44 kHz for 13.33 s by a 24 bit A/D converter (National Instruments). The digitized data were lowpass filtered at more than one-half of the sampling frequency.

Note that due to availability of the open jet wind tunnel at the ISVR, some of the aerodynamic measurements (not the noise) have to be carried out in another wind tunnel with a 0.5 × 0.5 m test sectional area. These measurements are related to the investigation of boundary layers on a sawtooth trailing edge of an untripped airfoil (in Sec. III.A) and the investigation of spanwise coherence of the airfoil wake produced by different sawtooth trailing edges (in Sec. V). Note that the angles of attack in these measurements were always set at a slightly higher $\theta = 5$ deg, thus they cannot be compared with the noise results directly. However, the main purpose of these aerodynamic tests is to provide supplementary data that can be used to explain the airfoil self-noise mechanisms that are subjected to nonflat plate serrated trailing edges.

III. Investigation of the Airfoil Boundary Layers

A. Boundary Layers on a Sawtooth Trailing Edge of an Untripped Airfoil

To test the hypothesis that a sawtooth trailing edge can trigger a bypass transition of the boundary layer into turbulence, thereby suppressing the separation bubble, and hence, the generation of tonal instability noise, a sawtooth trailing edge (S3 type, see Table 1) was affixed to the NACA 0012 airfoil main body as shown in Fig. 1. By adjusting the airfoil to θ = 5 deg and the freestream velocity running at U = 15 ms^{-1}, a hot wire was used to measure the airfoil's pressure surface boundary-layer profiles at five streamwise locations from upstream of the root of the serration, x/C = 0.83, to exactly the root of the serration, x/C = 0.87, and to three positions downstream, x/C = 0.90, 0.93, and 0.97. The measurement was repeated for a sharp trailing edge (S0). A comparison of the boundary-layer profiles on the sharp and sawtooth trailing edges is shown in Fig. 5. Note that U_0 in the abscissa of the figures refers to the local freestream velocity.

At upstream of the serration root, $x/C \leq 0.87$, both the mean and root mean square (rms) velocity profiles are found to be nearly identical. Further downstream, situated on the serrated portion of the airfoil, the mean and rms velocity profiles for the sawtooth trailing edge differ significantly from the sharp-edged case especially in the near-wall region, in which greater velocity excess and turbulence intensity are observed. This implies that the boundary layers on the sawtooth surface are more turbulent in character. These results have two important implications. First, the separation bubble is likely to be suppressed near a sawtooth trailing edge, and, therefore, the T–S instability waves will interact with a locally turbulent boundary layer, thereby removing the conditions required for the generation of boundary-layer instability tonal noise. Second, the fact that the mean and fluctuating boundary-layer profiles are similar at $x/C \leq 0.87$ would demonstrate that the serrations formed by cutting directly into the airfoil body do not significantly affect the upstream flowfield.

As mentioned before, the above experiment was carried out in a wind tunnel with a closed test section, which is different to the open jet wind tunnel used for the noise test. Although the boundary-layer results at θ = 5 deg presented in this subsection cannot be correlated with the noise results in Sec. IV per se, they can be used to confirm that the addition of serrations introduces bypass transition within the sawtooth region.

B. Development of Boundary Layers with and Without Artificial Tripping

Turbulent boundary layers were artificially generated by placing rough sandpaper near the leading edge ($x/C \approx$ 0.2) on both the suction and pressure surfaces. The variation in the boundary-layer surface pressure spectra S_{qq}, as measured by microphones embedded into the airfoil at x/C = 0.64 on both the suction and pressure surfaces of the airfoil, are presented in Figs. 6a–6b. Also included in the figures are the corresponding surface pressure spectra S_{qq} without the boundary-layer trips. Note that these results were obtained in the open jet wind tunnel, in which the airfoil incidence was adjusted to θ = 4.2 deg at U = 26.7 ms^{-1}.

The surface pressure spectra S_{qq} plotted in Fig. 6a resemble that of turbulent-like boundary layer with the characteristic high-frequency decay rate of approximately f^{-5}, even in the absence of the tripping tape on the suction

surface. The various peaks in the spectral around 1 kHz for the untripped case are due to boundary-layer instability noise radiating to the far field, which are then detected by the surface pressure sensors. In Fig. 6b, S_{qq} differ considerably at the pressure surface. Without the use of the boundary-layer trip, S_{qq} is of a comparatively lower level and less smooth than when tripping is applied. However, the boundary layer becomes turbulent when the trip is introduced as manifested by the considerably higher wall pressure spectrum level.

In conclusion, boundary layers at both the suction and pressure surfaces are turbulent near the trailing edge when tripping elements are applied on their respective surfaces. Without tripping, the boundary layer at the pressure surface is laminar (or separated) near the trailing edge. On the suction surface, the boundary layer may become turbulent near the trailing edge without the use of tripping tape. Figures 7a–7b show the sound pressure level (SPL) spectrum of the airfoil self-noise with the S0 trailing edge measured at Θ = 90 deg for the untripped and tripped cases, respectively, for mean flow velocities in the range of U = 20–60 ms^{-1}. The spectrum for the untripped case is characterized by numerous tones (Fig. 7a). On the other hand, no tones are present for the tripped case, in which broadband self-noise (Fig. 7b) is the dominant mechanism. Further details can be found in [11].

C. Laminar Separation Near the Trailing Edge of an Untripped Airfoil

A hot-wire probe is generally incapable of detecting reverse flow. The application of the surface-mounted thin-film arrays for the detection of a separated boundary layer has been documented by many researchers in the past [18–20]. The thin-film array technique was also employed in the current work in order to identify the separation boundary layer on the pressure surface of the sharp-edged (S0) untripped airfoil. The experiment was performed in the ISVR open jet wind tunnel under exactly the same setup and configuration as the noise test. The airfoil incidence is also set at θ = 4.2 deg.

Figure 8 represents the simultaneously measured time variation of the thin-film raw signals, the phase angles σ between HF1–HF2, HF2–HF3, and so on, as well as their corresponding coherence functions γ^2. These results correspond to U = 40 ms^{-1}. The arrows in the figures indicate the frequency that corresponds to the most dominant radiated instability tone noise. In a qualitative comparison of the thin-film raw signals, there are many instances when the raw signals between HF2–HF3 are in antiphase, which suggest that flow reversal might occur in the neighborhood of these thin films.

The cross spectrum between two thin-film signals $e_i(t)$ and $e_j(t)$ is a complex function, and it can be represented by $\left|\Phi_{e_i e_j}(f)\right| \exp\left(i\sigma_{e_i e_j}(f)\right)$, where $\sigma_{e_i e_j}(f)$ is the phase angle between coherent components of the thin-film signals $e_i(t)$, and $e_j(t)$. If we consider that i is the upstream thin film and j is the downstream thin film, the predominantly sinusoidal T–S instability waves that propagate past these sensors in the direction of the main flow should yield a positive phase angle σ at a frequency range that corresponds to the boundary-layer instability. This is indeed true for the phase spectrum of the HF1–HF2 case at 2.3 kHz < f < 2.8 kHz when sufficiently high coherences are achieved. The close spectral frequency relationship between the total T–S wave amplification factor and the radiated tonal instability noise has been documented in [11]. This relationship is further manifested in Fig. 8, in which the

frequency of the radiated tonal instability noise also coincides with the frequency range that corresponds to the high coherence of the thin-film signals at 2.3 kHz < f < 2.8 kHz.

However, the phase angles σ for the HF2–HF3 case have a negative sign at the similar frequency range. This implies that HF3 actually detects the coherent part of the signals ahead of HF2, which further indicates that flow reversal at the near-wall region has occurred there. Similarly, negative σ is also demonstrated for the HF3–HF4 case. A physical explanation for the thin-film results is proposed here: First the T–S wave is convecting from HF1 to HF2, in which the onset of the boundary-layer separation is located at around the location of HF2. The T–S wave then enters the bubble, detaches from the surface, and interacts strongly with the separating shear layer above the wall [9,10]. As it further propagates downstream, the near-wall flow reversal of the bubble will transport some of the oscillatory disturbances originated from the T–S instability wave from HF3 back to HF2, thus resulting in a reverse phase shift as interpreted from the near-wall thin-film signals. In summary, the phase change of the convective T–S instability wave has been used for the determination of flow separation.

Based on the above results, we confirm that the boundary layer at the airfoil's pressure surface separates at around x/C = 0.83. This location is slightly upstream at x/C = 0.87, which is the location for the root of the S1, S2, and S3 serrated trailing edges. However, the separation point of the boundary layer is considerably far from the root of the S2* serrated trailing edge (x/C = 0.93). The implication of the distance between the separation point and the location of the serration root to the level of airfoil tonal instability noise reduction will be discussed in the next section.

IV. Noise Results

This section presents the noise reduction performance of the sawtooth trailing edges S1, S2, S3, and S2* measured in the anechoic chamber under a free-field condition. Assuming the cylindrical spreading of waves from the airfoil trailing edge, the sound power level (PWL) radiated per unit span in the range of angles between 50 deg < Θ < 110 deg can be approximated by

$$W(f) = \frac{2\pi r \int S_{pp}(\mathrm{f},\Theta)\, d\Theta}{\rho c_o}, \qquad \mathrm{PWL}(f) = 10\log_{10}\left[W(f)/W_{ref}\right], \qquad 50^0 < \Theta < 110^0 \tag{2}$$

where S_{pp} (f, Θ) is the measured acoustic pressure PSD at a polar angle Θ. Definitions of other symbols in Eq. (2) are listed in the nomenclature. Examples of the variation of the PWL with frequency for the airfoil instability tonal noise (untripped) and broadband noise (tripped) are shown in Figs. 9a–9b. The figures demonstrate that airfoil trailing-edge serrations cut into the main body of the airfoil has a substantial effect on the sound power spectra, which differs considerably depending upon whether the boundary layer is laminar or turbulent. As discussed earlier, the obvious disadvantage with the use of serrations cut into the airfoil body is that it will inevitably generate narrowband noise due to vortex shedding from the blunt part of the serration at the root as shown in Fig. 9b. At frequencies above the shedding frequencies, it was found that about 3 dB reductions in the broadband level can be

observed. As the following subsections will demonstrate, the impact of bluntness noise can be reduced while retaining the broadband noise benefits at other frequencies by the appropriate choice of serration parameters.

A. Boundary Layer Instability Tonal Noise Reduction by Trailing Edge Serrations

The difference in sound power level ΔPWL between a baseline straight trailing edge (S0) and a serrated trailing edge (S1, S2, S3, or S2*) airfoil was computed from

$$\Delta\mathrm{PWL} = \mathrm{PWL}_{baseline} - \mathrm{PWL}_{serration}\ , \tag{3}$$

Figures 10a–10d shows the color maps of ΔPWL as a function of frequency and mean velocity for the serrated trailing edges S1, S2, S3, and S2*, respectively, for the untripped case, in which T–S instability tonal noise is dominant. By comparing S1–S3 (same $2h$ and ε but different φ and λ/h), instability tonal noise reductions in excess of 30 dB are observed. The reason for this reduction can be explained by the fact that the separation region, commonly believed to be a prerequisite for the T–S wave instability tonal noise, is situated close to the trailing-edge serrations. Experimental results obtained by the surface-mounted thin-film array technique in Sec. III.C suggest that boundary-layer separation occurs at around x/C = 0.83 at the pressure surface. Because the root of the sawtooth is situated at x/C = 0.87 for the S1–S3 cases, a large portion of the otherwise separation region is not expected to be present within the sawtooth surface. Therefore, the incoming T–S waves cannot be amplified sufficiently for the radiation of instability tonal noise to occur.

Further evidence for the necessary role of a separation bubble for T–S instability tonal noise to occur is found in the ΔPWL contours for the S2 and S2* cases (same φ and λ/h but different $2h$ and ε). Because the root of the sawtooth for the S2* case is situated at x/C = 0.93, boundary-layer separation is only partially suppressed, and there are still some partial interactions between the separated shear layer and the incoming T–S waves upstream of the sawtooth. As a result, the boundary-layer instabilities can still scatter into noise at the root of the sawtooth, although it is less efficient compared to the baseline S0 case. The corresponding level of ΔPWL reduction for the S2* case is the smallest, and several tonal "rungs" are still discernible in the noise spectrum in Fig. 10d (indicated by the arrows). The presence of these rungs suggests that certain tone frequencies, in relation to the T–S waves, are preselected up stream of the trailing edge in accordance with the hypothesis proposed by McAlpine et al. [9].

The effect of serration angle φ (or λ/h) on the instability tonal noise reduction is demonstrated in Figs. 10a–10c. The serration with the largest angle φ can be seen to produce the largest reduction in the instability tonal noise. For smaller serration angles φ, narrowband vortex shedding noise can be seen to increase as a result of root bluntness at frequencies below the T–S instability tonal noise (e.g., Fig. 10a for the S1 case). For the serration with the largest φ (S3), bluntness-induced noise is nonexistent as shown in Figs. 9a and 10c.

The overall sound power level (OAPWL) of the airfoil noise at a particular flow velocity can be defined as

$$\mathrm{OAPWL} = 10\log_{10}\left[\int W(\mathrm{f})\,d\mathrm{f}\,/\,W_{ref}\right], \tag{4}$$

In this study, OAPWL was obtained by integrating the sound power over the frequency range, 0.1–15 kHz, with the lower bound limit representing approximately the cutoff frequency of the anechoic chamber. Figure 11a shows the

variation of OAPWL with mean velocity U for the various serrated trailing edges. Initially the OAPWL for S0–S3 and S2* remain near constant in the speed range, U = 20–24 ms^{-1}, where the instability tonal noise is absent. For the S0 sharp trailing edge, instability tonal noise begins to occur in the speed range U = 24–30 ms^{-1}. From U = 30–60 ms^{-1}, instability tonal radiation continues to be dominant with a speed dependence of $W_{(S0)} \propto U^5$, corresponding to classical trailing-edge noise radiation. In this velocity range, the spectrum is characterized by numerous and equally spaced discrete frequencies (sometimes as many as 10 at a single velocity). Identical behavior is found in the experimental and numerical works [11–13,21,22]. For the S1–S3 serrations, there is no sudden jump in OAPWL in the speed range, U = 20–60 ms^{-1}, and it is found that $W_{(S1,\ S2\ \text{and}\ S3)} \propto U^7$. The change in the velocity power law from 5 to 7 demonstrates that noise radiation at the trailing edge has largely been inhibited, and the dominant noise source now mainly arises from quadrupole sources in the jet, as well as the airfoil wake. For the S2* serration, the overall sound power also scales with U^5 from $U \approx$ 40–60 ms^{-1}. This is because some lower level instability tonal noises have been known to exist for this type of serration within this velocity range.

The main source of uncertainty for the above result is that the calculation of the overall sound power by Eq. (4) may include the contribution from the leading-edge noise. The leading-edge noise usually occurs at low frequencies, and it is well separated from the trailing-edge noise, which occurs at a higher frequency range. The very low residual turbulence level in the free jet provided by the open jet wind tunnel also minimizes the turbulence leading-edge interaction noise in the current study. Based upon substituting different values of the lower frequency limit in the OAPWL calculation, it is estimated that the uncertainty of the velocity power law varies within ±0.5. This level of uncertainty also applies to the tripped airfoil case, which will be presented in the next subsection.

The difference in the OAPWL, ΔOAPWL, between a baseline straight trailing edge (S0) and a serrated trailing edge (S1, S2, S3, or S2*) was calculated from

$$\Delta\text{OAPWL} = \text{OAPWL}_{\text{baseline}} - \text{OAPWL}_{\text{serration}} \tag{5}$$

In this case a positive ΔOAPWL represents overall sound power reduction, and vice versa. As shown in Fig. 11b, appreciable sound power reductions occur at U > 24 ms^{-1} with levels of noise reduction up to 17 dB. By comparing serrations S1–S3 of the same 2h but different φ and λ/h, the level of sound power reduction increases as φ or λ / h increases. For the pair of serrations S2 and S2* with the same φ and λ / h but different 2h, a larger level of sound power reduction is achieved by the serrated trailing edge with the longer serration length 2h, because more of the boundary-layer separation region has been affected in this case.

B. Broadband Noise Reduction by Trailing Edge Serrations

Figures 12a–12d shows the color maps of ΔPWL as a function of frequency and mean velocity for the serrated trailing edges S1, S2, S3, and S2*, respectively, when boundary-layer tripping is applied on both of the suction and pressure surfaces. Note that the range of color scale adopted in this figure (±20 dB) is smaller than the range adopted in Fig. 10 (±30 dB). Moderate reductions in sound power level in broadband noise have been achieved by the serrated trailing edges. By comparing ΔPWL for the S1–S3 serrations, the level of noise reduction is found to increase when φ or λ / h is reduced, which is consistent with the findings of [1–3,7] in which flat plate inserts were

used (but in contrast with the instability tonal noise reduction discussed in Sec. IV.A). One important feature demonstrated by these nonflat plate serrations is that they show better noise performance at a high frequency than when flat plate inserts were used [1,2], which always increases noise radiation. As expected, although noise is reduced over most of the frequency range, the noise is increased over a very narrow frequency band caused by the bluntness at the serration root. This issue will be further discussed in the next paragraph. The narrowband vortex shedding noise level decreases as φ (or λ/h) is increased. On the other hand, by comparing the S2 and S2* serration cases with the same serration angle φ but different lengths $2h$ (and hence different bluntnesses ε), the longer serration with a greater bluntness would produce a higher amplitude vortex shedding noise at a lower frequency.

To investigate the mechanism responsible for the narrowband vortex shedding noise generation, a separate NACA 0012 airfoil of a 200 mm chord was manufactured with an identical S3 trailing-edge serration geometry, which is scaled to yield the same $2h/C$ value. Flow visualization tests were performed in water at a low speed of 0.04 ms^{-1}, corresponding to a Reynolds number of approximately 0.9×10^4 based on the chord length. The choice of the low speed is because a reasonably clear vortex shedding pattern can only be discernible at around this speed region. Although the Reynolds number for this hydrodynamic test is generally lower than the noise results presented in this paper, the airfoil was tripped to produce a turbulent-like boundary layer at the trailing edge roughly equivalent to the turbulent noise source generated in the noise test. This airfoil was positioned at $\theta = 5$ deg with respect to the mean flow direction in a water tunnel with a 300 × 450 mm cross-sectional area. Blue color dye was injected at a constant flow rate near the root of one of the sawtooths as shown in Fig. 13. In the figure, snapshots of six time frames (Δt = 0.375 s) are shown. The filled arrows represent upwash flow (pressure surface → suction surface) within a sawtooth gap; the nonfilled arrows represent downwash flow (suction surface → pressure surface) within a sawtooth gap. Flow in the vicinity of the sawtooth is characterized by a periodic oscillatory motion of the upwash and downwash of the blue dye at a frequency of about 1.3 Hz. If this frequency is scaled with the bluntness of the serration root ε, the resulting hydrodynamic Strouhal number is about 0.19. This value compares reasonably well with the Strouhal numbers for the narrowband vortex shedding noise produced by the S3 case, which are in the range from 0.14 to 0.17, depending slightly upon the flow speed and angle of attack (to be discussed in Sec. V). Therefore, there is strong evidence that the vortex shedding noise is produced by the periodic oscillation of flow within the sawtooth gap.

The variations of OAPWL with a mean flow velocity for the S0–S3 and S2* trailing-edge serrations are shown in Fig. 14a. In nearly all cases, the sound powers scale with the sixth power of the flow velocity. This velocity dependence is usually associated with vortex shedding noises from bluff bodies [23] and an airfoil with a blunt trailing edge [17]. For the S0 baseline case, we also have observed a velocity scaling of $W_{(S0)} \propto U^{5.5–6}$, which is higher than the fifth power scaling observed previously. This indicates that although acoustic radiation from the trailing edge is still the dominant mechanism, other noise sources (e.g., the leading-edge noise) might slightly contribute to the OAPWL, especially in the higher velocity region. In terms of the overall sound power reduction ΔOAPWL as shown in Fig. 14b (similarly, a positive ΔOAPWL represents overall sound power reduction, and vice versa), the S1 serrated trailing edge produces a higher noise level than the S0 baseline case across the whole velocity range owing to the dominance of the vortex shedding noise. For the other serrations S2 and S3, the level of the

vortex shedding noise decreases when the serration angle φ (or λ / h) is large. Therefore, the S2 serrated edge produces ΔOAPWL that varies between an increase and a reduction across the velocity range, whereas the S3 serrated edge consistently reduces the noise relative to the S0 baseline case, especially at higher velocities. The level of the vortex shedding noise is also found to decrease with the reduced bluntness value ε. This behavior is clearly observed in Fig. 14b, showing larger overall sound power reductions for the S2* serration compared to its S2 counterpart.

V. Discussion of Noise Results

Reducing airfoil self-noise through the use of trailing-edge serrations cut into the airfoil body has been investigated experimentally in this paper. The use of a trailing-edge serration to suppress both instability tonal noise in the case of a laminar boundary layer and broadband noise in the case of a turbulent boundary layer has been demonstrated. When the T–S waves convect across the airfoil surface (especially at the pressure surface) and are amplified by a laminar separation region, instability tonal noise of high intensity will be radiated near the trailing edge. The use of serrations on the trailing edge has been found to be highly effective in suppressing instability tonal noise. Based on the data presented here, the serration triggers the local boundary layer into a turbulent state, thus minimizing the size of the separation region, and hence, removing the requisite condition for T–S instability tonal noise. Although cutting serration into the airfoil body introduces bluntness at the serration root, no significant narrowband vortex shedding noise radiation has been observed. This implies that the wake flow for an untripped airfoil is characterized by a weak vortex shedding. We note the absence of vortex shedding for a blunt trailing edge in [24], when the boundary layers on the airfoil's suction surface and pressure surface are different, that is, one is turbulent and another one is laminar. A similar phenomenon is also reflected in the untripped wall pressure spectra. It was found that the boundary layer at the pressure surface is non-turbulent near the trailing edge, whereas for the suction surface, the boundary layer is turbulent near the trailing edge (see Figs. 6a–6b). The different states of boundary layers on the suction and pressure surfaces near the trailing edge can apparently prevent the formation of longitudinal vortex shedding in the near wake immediately after the serration root.

However, if the boundary layers on the suction and pressure surfaces are both turbulent (tripped airfoil), the sound power level produced by the vortex shedding will be significant for narrow angle (small φ) serrated trailing edges. The exact mechanism responsible for the generation of vortex shedding for a nonflat plate-type serrated trailing edge, when both of the suction and pressure surfaces are turbulent, remains a subject of investigation, and this is not pursued in the current paper. As shown in Figs. 12a–12c for the ΔPWL contours, the narrowband frequencies f_d corresponding to the vortex shedding frequencies differ from the serrated groups S1, S2, and S3, which all share the same root bluntness ε. Figure 15 is a plot of the Strouhal frequency for the vortex shedding noise ($f_d\varepsilon / U$), defined with respect to the bluntness ε and flow velocity U, suggesting that there is no universal Strouhal number dependency for the S1, S2, and S3 cases. If an airfoil has a two-dimensional blunt trailing edge, whose ε is constant across the airfoil span and has the same value as the S1, S2, and S3 cases, the corresponding Strouhal

numbers ($f_d\varepsilon / U$) are predicted to be constant with the flow velocity [17]. The measured Strouhal numbers for the S1, S2, and S3 cases are found to vary between $U^{0.1}$ and $U^{0.15}$.

Flow passing through a sawtooth region could be highly three dimensional in nature. When the airfoil is set at an angle of attack, the static pressure difference across the suction and pressure surfaces will force the flow to wrap around each of the sawtooth side edges in a manner similar to the wingtip vortices of a three-dimensional airfoil. Note that this type of spanwise secondary flow is different with the longitudinal vortices that are shed from the blunt serration roots. The possible interaction between the secondary flow with the longitudinal vortices has been shown to significantly affect the coherence of the vortex shedding street in the wake flow. To quantify this effect, the spanwise coherences γ^2 of the airfoil wake turbulence velocity for three types of trailing edges, S2, S3, and SB, were measured at θ = 5 deg in a closed-section wind tunnel. Here, SB is a two dimensionally blunt, nonserrated trailing edge with the same bluntness ε as the S2 and S3 serrated trailing edges. The spanwise coherence γ^2 is defined as

$$\gamma^2 = \frac{\left|\Phi_{v_i v_j}(f)\right|^2}{\Phi_{v_i v_i}(f)\Phi_{v_j v_j}(f)}\ , \tag{6}$$

where $0 \le \gamma^2 \le 1$. $\Phi_{v_i v_j}(f)$ is the cross spectrum between the two streamwise fluctuating velocity signals v_i and v_j. The velocity measurement v_i was measured by a single hot wire situated at a fixed, stationary position of x = 15 mm downstream of the sawtooth tip or (15 + 2h) mm behind the SB blunt trailing edge. The velocity measurement v_j was measured by another single hot wire situated at the same downstream x position but was traversed along the spanwise z direction. $\Phi_{v_i v_i}(f)$ and $\Phi_{v_j v_j}(f)$ are the autospectra of each individual fluctuating velocity signal. Both hot-wire probes are of the DANTEC 55P11 type (5 μm in diameter and a 1.25 mm length). The overheat ratios were set at a slightly lower value of 1.6 to minimize thermal interference between the wires when they are close to each other. The hot-wire signals were digitized at a sampling rate of 20 kHz.

The results of γ^2 for the SB, S2, and S3 cases in a tripped airfoil are shown in Fig. 16. Each figure is accompanied by a sketch on the left hand side to illustrate the serration/blunt geometries. The symbols '*b*', '*r*' and '*t*' denote 'blunt', 'root' and 'tip' respectively. The stationary, reference point for the γ^2 function is situated at z = 0. Note that the γ^2 function here is a measure of the spanwise coherence of the longitudinal vortex shedding. Strong spanwise coherence can be observed for the SB case, which clearly indicates that the wake flow is mainly characterized by longitudinal vortex shedding. For the S2 serrated case, the spectral frequency is broader than the SB case with a reduced spanwise coherence level. The wake flow emanated from the root region, although still predominantly characterized by longitudinal vortex shedding, is already affected considerably by the secondary flow. As expected, there is also no coherence between each successive sawtooth. For the S3 serrated trailing edge, an overall very low-spanwise coherence level is observed. This indicates that the wake flow is highly three-dimensional in this case, in which the serration angle φ is the largest.

For the case of low φ (or λ / h), the total number of serration "blunt roots" per unit span is increased. This tends to reduce the strength of the spanwise secondary flow, whereas the longitudinal vortex shedding (caused by the bluntness at the root region) is expected to be considerably coherent. This is manifested in the sound power spectra

in Figs. 12a–12c, in which it can be seen that the sound power of the narrowband vortex shedding noise increases as φ decreases. It also explains that the Strouhal number, which corresponds to the narrowband frequencies produced by a trailing edge with a "full" two-dimensional bluntness ($\varphi = 0$), tends to agree better with those produced by a serrated trailing edge of low φ as demonstrated in Fig. 15. Conversely, for a trailing edge with a larger serration angle (e.g., the S3 case), the more prominent secondary flow is expected to interact more strongly with the longitudinal vortex shedding. This process leads to a modification to the narrowband frequency and also reduces its sound power level. Based on this behavior, we can conclude that, as far as a tripped boundary layer is concerned, a serrated trailing edge with large serration angle φ would produce a lower level of the vortex shedding noise.

However, the overall noise performance of a serrated trailing edge also depends on the level of broadband noise reduction. We now consider the performance of the serrations in three frequency bands as defined in Figs. 12a–12b:

1) Frequency band I: the entire frequency band is to deduce the "overall" performance: $0 < f < \infty$ or $J = (0, \infty)$.
2) Frequency band II: the frequency bandwidth corresponding to that in which the sound power is reduced compared to the baseline case (S0): $f < f_1$ and $f > f_2$ or $J = (0, f_1) \cup (f_2, \infty)$.
3) Frequency band III: the frequency bandwidth corresponding to that in which the sound power is increased compared to the baseline case (S0): $f_1 < f < f_2$ or $J = (f_1, f_2)$.

Here, f_1 and f_2 denote the lower and upper frequency limits within which vortex shedding noise due to bluntness at the trailing edge is significant. Both f_1 and f_2 increase with the mean flow speed as depicted in Fig. 12. In each frequency band (I, II, and III), an overall noise performance metric (NPM) is given by

$$NPM = 10\log_{10}\left(\int_{f\in J} W_{baseline}df \Big/ \int_{f\in J} W_{serration}df\right), \tag{7}$$

Figure 17 shows the variation of NPM versus φ across $U = 20 - 60$ ms^{-1}. Note that positive NPM represents sound power reduction and vice versa. The serrated trailing edges investigated here all have the same $2h$ and ε. By examining the variations of sound power reductions (frequency band II), maximum sound power reduction of up to 6.5 dB is achievable within the range of serration angle φ investigated here. Sound power increase (frequency band III) caused by the serration bluntness is most significant at small values of φ but reduces as φ increases (we note that it is possible to further reduce the narrowband tonal noise level by employing woven wire mesh screen across the sawtooth gaps to reduce the bluntness induced vortex shedding [25]). Finally, by examining the overall sound power reduction across the entire bandwidth (frequency band I), it can be seen that an overall reduction across all frequencies is only achieved for the serration with the largest φ. Because the amount of sound power reduction (frequency band II) is relatively insensitive to φ in comparison to the sound power increase (frequency band III), the optimum serration geometry, as far as the nonflat plate type is concerned, is thus limited by the narrowband noise radiation due to the vortex shedding (frequency band III). Serration S3 with the largest φ therefore gives the best noise performance overall. This criterion for the reduction of the airfoil broadband noise, coincidently, also applies to the untripped boundary layer case from which the instability tonal noise is dominant.

VI. Conclusion

This paper reports an experimental study on the aeroacoustic properties of several nonflat plate-type serrated trailing edges of an airfoil. The use of this particular type of serrated trailing edge could offer better structural stability over the flat-plate insert type. The objective of this paper is to investigate whether it is feasible to employ these nonflat plate-type serrated trailing edges to reduce both the instability tonal noise and broadband noise produced by the trailing edge of an airfoil.

When an untripped NACA 0012 airfoil is set at $\theta = 4.2$ deg, and the flow velocity was tested up to 60 ms^{-1} ($Re = 6 \times 10^5$ based on the chord length), a detailed inspection of the sound power spectra shows that by using the serrated trailing edge, sound power reduction of more than 30 dB (or up to 20 dB for the ΔOAPWL) for the mainly boundary-layer instability tonal noise radiation can be achieved. In addition, there is no significant noise penalty from the radiation of the vortex shedding near the blunt root of the sawtooth trailing edge. Based on the results obtained in this study, several important criteria for an effective boundary-layer instability tonal noise reduction by a serrated trailing edge are summarized below:

1) To maximize the impact of the serrations, the boundary-layer separation should occur at a location near the sharp edge of the otherwise nonserrated trailing edge. The serration length ($2h$) of the sawtooth should be compatible with the boundary-layer separation length.
2) The serration angle (φ) should be sufficiently large.

When the airfoil surfaces are tripped such that turbulent boundary layers are generated at both of the suction and pressure surfaces, the radiated noise spectra will be dominated by broadband noise of a much lower sound power level than the instability tonal noise. The sound power reduction of the broadband noise of up to 6.5 dB (in the noise performance metric [NPM] band II) by the serrated trailing edges has been observed. Another very important result is that the use of the nonflat plate-type serrations has better noise performance at a high frequency than serration by flat-plate inserts [1,2]. However, noise increase caused by the vortex shedding from the blunt roots is also more significant in this case. The level of the narrowband vortex shedding noise will reduce when a large serration angle (φ) is used because of the greater flow mixing near the blunt roots. In conclusion, moderate self-noise reductions can still be achieved by the nonflat plate-type serrated trailing edge if the following conditions are fulfilled:

1) The serration angle (φ) is sufficiently large. Note that our results also agree with Gruber et al. [1] and Howe [7] in that maximum broadband noise reduction would require a smaller φ. However, the recommendation of a large φ in this paper for the broadband noise reduction is based on the consideration of minimizing the narrowband vortex shedding noise.
2) The serration length ($2h$) of the sawtooth should be equal to or greater than the turbulent boundary-layer thickness. For a nonflat plate-type serration, a slightly smaller $2h$ is also desirable, because it will generate a lower level of the narrowband vortex shedding noise due to the smaller bluntness (ε).

In conclusion, the use of nonflat plate-type serration can be effective and versatile in reducing airfoil self-noise. This study provides the scope for further works to improve the industrial worthiness of the serration technology, as well as the understanding of the broadband noise mechanisms. The noise performance of the nonflat plate serrated trailing edge should also be investigated for airfoils with different geometry and angle of attack. One of the sensible

paths for the continuation of the current work is to develop methodologies to inhibit the strength of the vortex shedding flow produced by the partial blunt roots.

Acknowledgment

This work is partly supported by the Brunel Research Initiative and Enterprise fund.

References

[1] Gruber, M., Joseph, P. F. and Chong, T. P., "On the Mechanism of Serrated Airfoil Trailing Edge Noise Reduction," *17th AIAA/CEAS Aeroacoustic Conference and Exhibit*, AIAA Paper 2011–2781, 2011, Portland, Oregon.

[2] Oerlemnans, S., Fisher, M., Maeder, T. and Korler, K., "Reduction of Wind Turbine Noise using Optimized Airfoils and Trailing Edge Serrations," *AIAA Journal*, Vol. 47, 2009, pp. 1470–1481.

[3] Moreau, D. J., Brooks, L. A. and Doolan C. J., "Flat Plate Self-Noise Reduction at Low-to-Moderate Reynolds Number with Trailing Edge Serrations," *Proceedings of Acoustics*, 2011, Gold Coast, Australia.

[4] Geyer, T., Sarradj, E. and Fritzsche, C., "Measurement on the Noise Generation at the Trailing Edge of Porous Airfoils," *Experiment in Fluids*, Vol. 48, 2010, pp. 291–308.

[5] Herr, M., "Design Criteria for Low-Noise Trailing-Edges," *13th AIAA/CEAS Aeroacoustic Conference and Exhibit*, AIAA Paper 2007–3470, 2007, Rome, Italy.

[6] Finez, A., Jondeau, E., Roger, M. and Jacob, M. C., "Broadband Noise Reduction with Trailing Edge Brushes," *16th AIAA/CEAS Aeroacoustic Conference*, AIAA Paper 2010–3980, 2010, Stockholm, Sweden.

[7] Howe, M. S., "Noise produced by a Sawtooth Trailing Edge," *Journal of the Acoustical Society of America*, Vol. 90, 1991, pp. 482–487.

[8] Lowson, M. V., Fiddes, S. P. and Nash, E. C., "Laminar Boundary Layer Aeroacoustic Instabilities," *32nd Aerospace Sciences Meeting and Exhibition*, AIAA Paper 1994–0358, 1994, Reno, Nevada.

[9] McAlpine, A., Nash, E. C. and Lowson, M. V., "On the Generation of Discrete Frequency Tones by the Flow around an Aerofoil," *Journal of Sound and Vibration*, Vol. 222, 1999, pp. 753–779.

[10] Nash, E. C., Lowson, M. V. and McAlpine, A., "Boundary-Layer Instability Noise on Airfoils," *Journal of Fluid Mechanics*, Vol. 382, 1999, pp. 27–61.

[11] Chong, T. P., Joseph, P. F. and Kingan, M. J., "An Investigation of Airfoil Tonal Noise at Different Reynolds Numbers and Angles of Attack," *Applied Acoustics*, Vol. 74, 2013, pp. 38-48.

[12] Desquesnes, G., Terracol, M. and Sagaut, P., "Numerical Investigation of the Tone Noise Mechanism over Laminar Airfoils," *Journal of Fluid Mechanics*, Vol. 591, 2007, pp. 155–182.

[13] Kingan, M. J. and Pearse, J. R., "Laminar Boundary Layer Instability Noise produced by an Aerofoil," *Journal of Sound and Vibration*, Vol. 322, 2009, pp. 808–828.

[14] Amiet, R. "Noise due to Turbulent Flow past a Trailing Edge," *Journal of Sound and Vibration*, Vol. 47, 1976, pp. 387–393.

[15] Jones, L. E. and Sandberg, R. D., "Direct Numerical Simulations of noise Generated by the Flow over an Airfoil with Trailing Edge Serrations," *15th AIAA/CEAS Aeroacoustic Conference and Exhibit*, AIAA Paper 2009–3195, 2009, Miami, Florida.

[16] Chong, T. P., Joseph, P. F. and Davies, P. O. A. L., "Design and Performance of an Open Jet Wind Tunnel for Aero-Acoustic Measurement," *Applied Acoustics*, Vol. 70, 2009, pp. 605–614.

[17] Brooks, T. F., Pope, D. S. and Marcolini, M. A., "Airfoil Self-Noise and Prediction," NASA Reference Publication-1218, 1989.

[18] Stack, J. P., Mangalam, S. M. and Berry, S. A., "A unique Measurement Technique to study Laminar-Separation Bubble Characteristics on an Airfoil," *19th AIAA Fluid Dynamics, Plasma Dynamics and Laser Conference*, AIAA Paper 1987-1271, 1987, Honolulu, Hawaii.

[19] Ida, F., Shinohara, J., Kunikyo, T., Nakasu, K. and Cook, S. C. P., "Experimental Quantitative Turbine Boundary-Layer Investigations using Multiple Hot Film Sensor," *18th AIAA Aerospace Ground Testing Conference*, AIAA Paper 1994-2537, 1994, Colorado Springs, Colorado.

[20] Lee, T. and Basu, S., "Measurement of Unsteady Boundary Layer Developed on an Oscillating Airfoil using Multiple Hot-Film Sensors," *Experiments in Fluids*, Vol. 25, 1998, pp. 108–117.

[21] Paterson, R., Vogt, P., Fink, M. and Munch, C., "Vortex Noise of Isolated Airfoils," *Journal of Aircraft*, Vol. 10, 1973, pp. 296–302.

[22] Arbey, H. and Bataille, J., "Noise Generated by Airfoil Profiles placed in a Uniform Laminar Flow," *Journal of Fluid Mechanics*, Vol. 134, 1983, pp. 33–47.

[23] Hutcheson, F. V. and Brooks, T. F., "Noise Radiation from Single and Multiple Rod Configurations," *12th AIAA/CEAS Aeroacoustic Conference and Exhibit*, AIAA Paper 2006–2629, 2006, Cambridge, Massachusetts.

[24] Sagrado, A. G., "Boundary Layer and Trailing Edge Noise Sources," PhD Thesis, University of Cambridge, 2007.

[25] Chong, T. P., Joseph, P. F. and Gruber, M., "Airfoil Self Noise Reduction by Non-Flat Plate Type Trailing Edge Serrations," *Applied Acoustics*, Vol. 74, 2013, pp. 607-613.

Table 1 Trailing edge serration geometries investigated in this study

Notation	φ (^{o})	2h (mm)	λ/h	ε (mm)
S0	-	-	-	-
S1	7	20	0.49	5.7
S2	12	20	0.85	5.7
S3	25	20	1.87	5.7
S2*	12	10	0.85	3.1

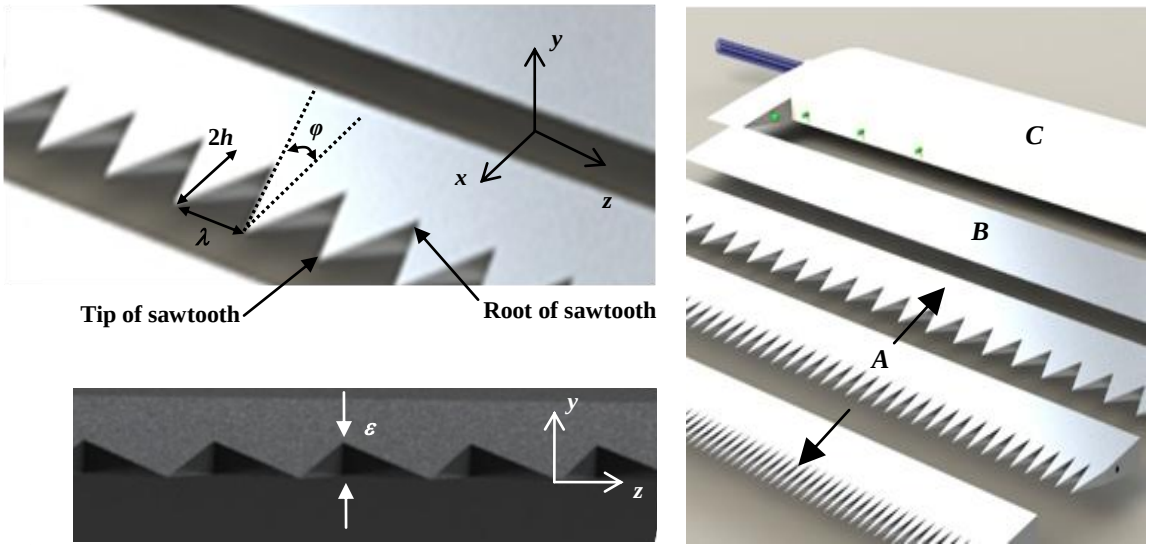

Fig. 1 Illustrations of a sawtooth geometry (left) and several nonflat plate serrated trailing edges (*A*), a sharp trailing edge (*B*) and an airfoil main body (*C*) used in the current study (right).

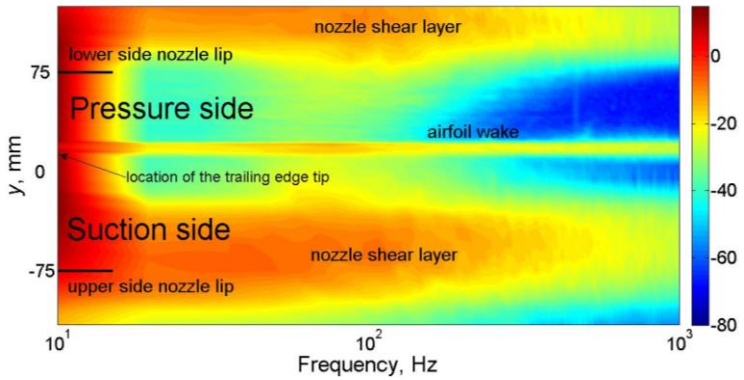

Fig. 2 Velocity PSD (m^2s^{-2}/Hz) contour map at 5 mm behind the S0 trailing edge at θ = 4.2 deg and U = 30 ms^{-1}.

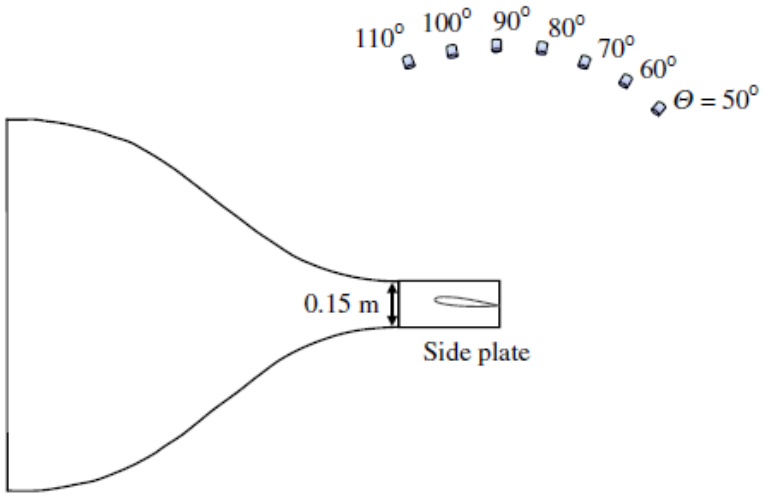

Fig. 3 Experimental set up for the aeroacoustic test of the airfoil noise. Seven far field microphones were set up at polar angle, Θ from 50 deg to 110 deg.

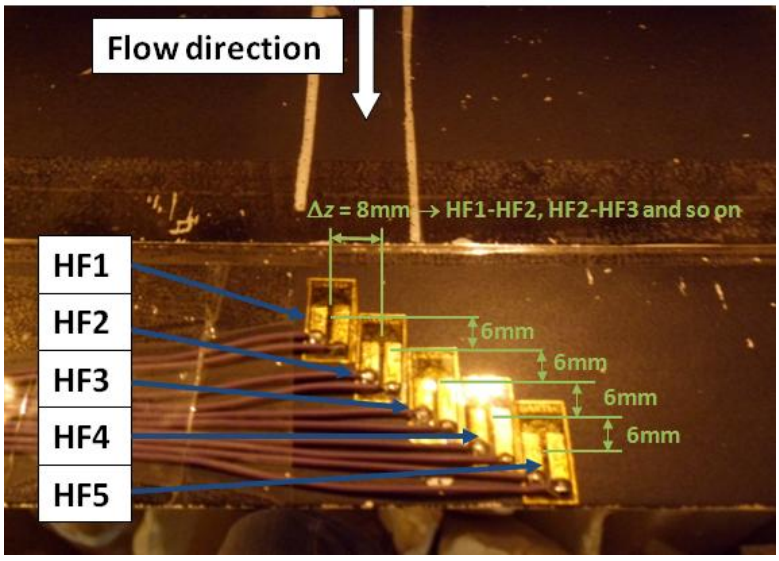

Fig. 4 Surface mounted thin film array for the detection of the separation boundary layer at the airfoil's pressure surface.

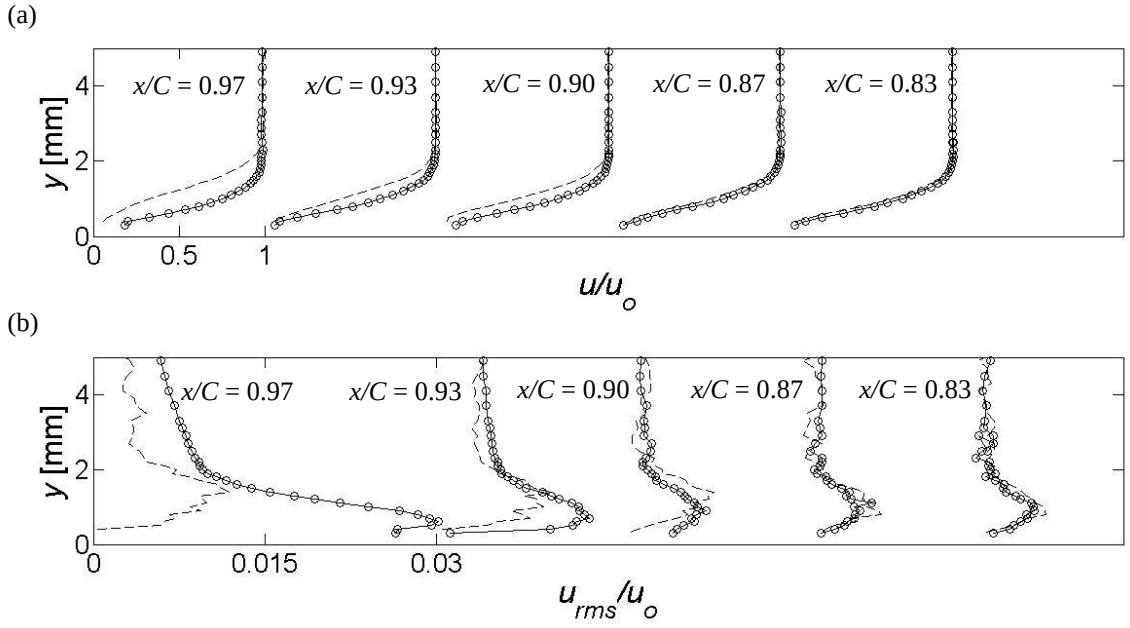

Fig. 5 Developments of the boundary layer: a) mean velocity and b) rms velocity fluctuation for the sharp S0 trailing edge (- - -) and serrated S3 trailing edge (–o–) at the airfoil's pressure surface at θ = 5 deg and U = 15 ms^{-1}.

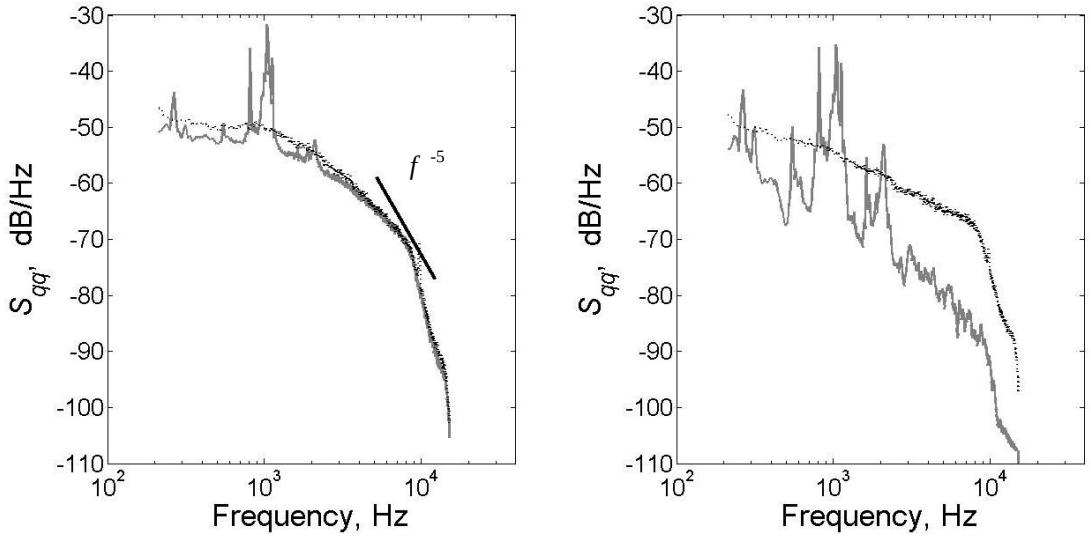

a) b)

Fig. 6 S_{qq} measured at θ = 4.2 deg and U = 26.7 ms^{-1} for the a) suction surface and b) pressure surface, both of which are at x/C = 0.64. The dotted lines (.....) and solid lines (—) represent S_{qq} with and without boundary layer tripping tapes, respectively, near the leading edge of the airfoil.

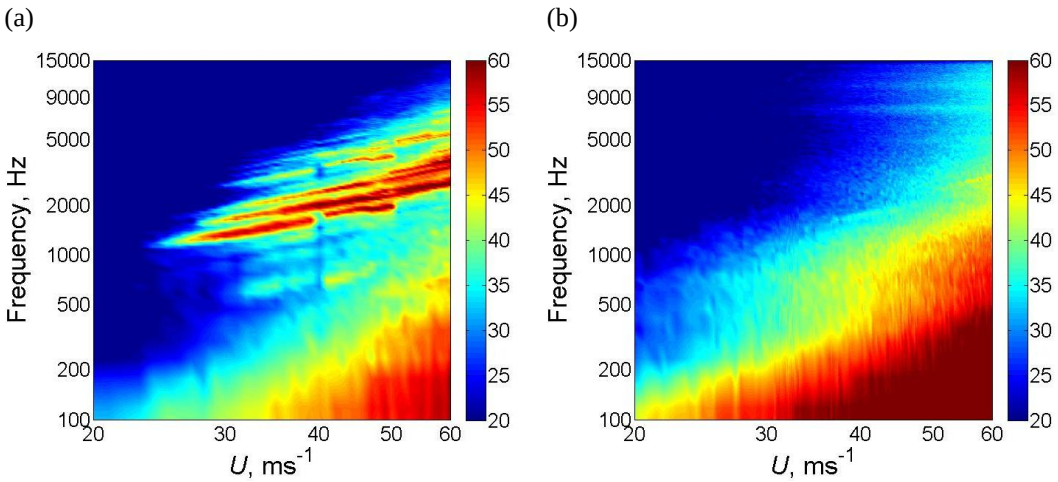

Fig. 7 Color maps of the Sound Pressure Level, decibel (with reference to 20 μPa) at 1 Hz bandwidth for the (a) untripped case and (b) tripped case. The airfoil is set at θ = 4.2 deg.

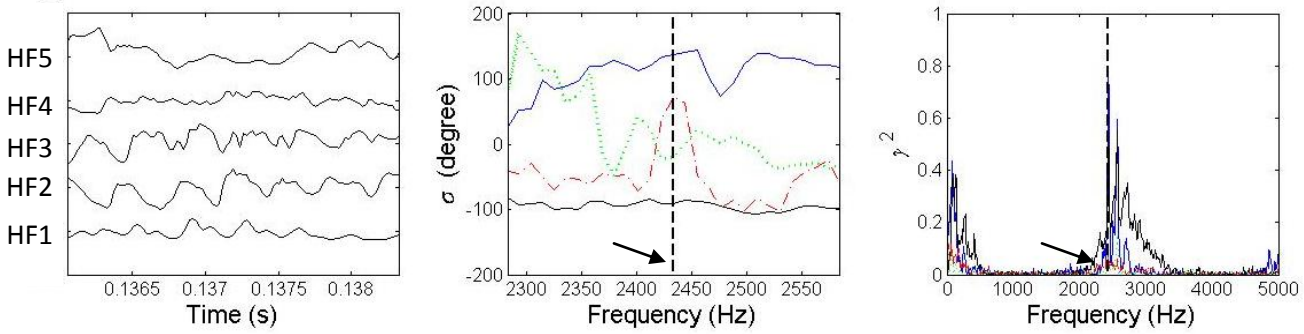

Fig. 8 Surface thin-film arrays raw signals, phase angles (σ) and coherences (γ^2) at θ = 4.2 deg and U = 40 ms^{-1}. HF1-HF2 (blue —), HF2-HF3 (black —), HF3-HF4 (red –•–) and HF4-HF5 (green •••••) in the σ and γ^2 spectral diagrams.

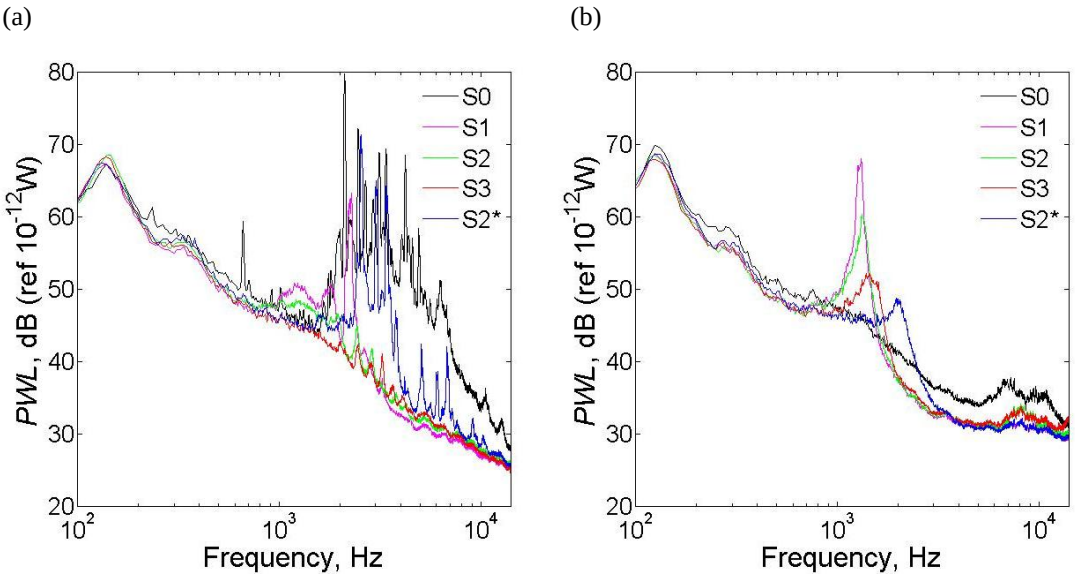

Fig. 9 Comparisons of the *PWL* spectra when boundary layers on both of the suction and pressure surfaces are (a). untripped at U = 54 ms^{-1}, and (b). tripped at U = 51 ms^{-1}. The airfoil is set at θ = 4.2 deg.

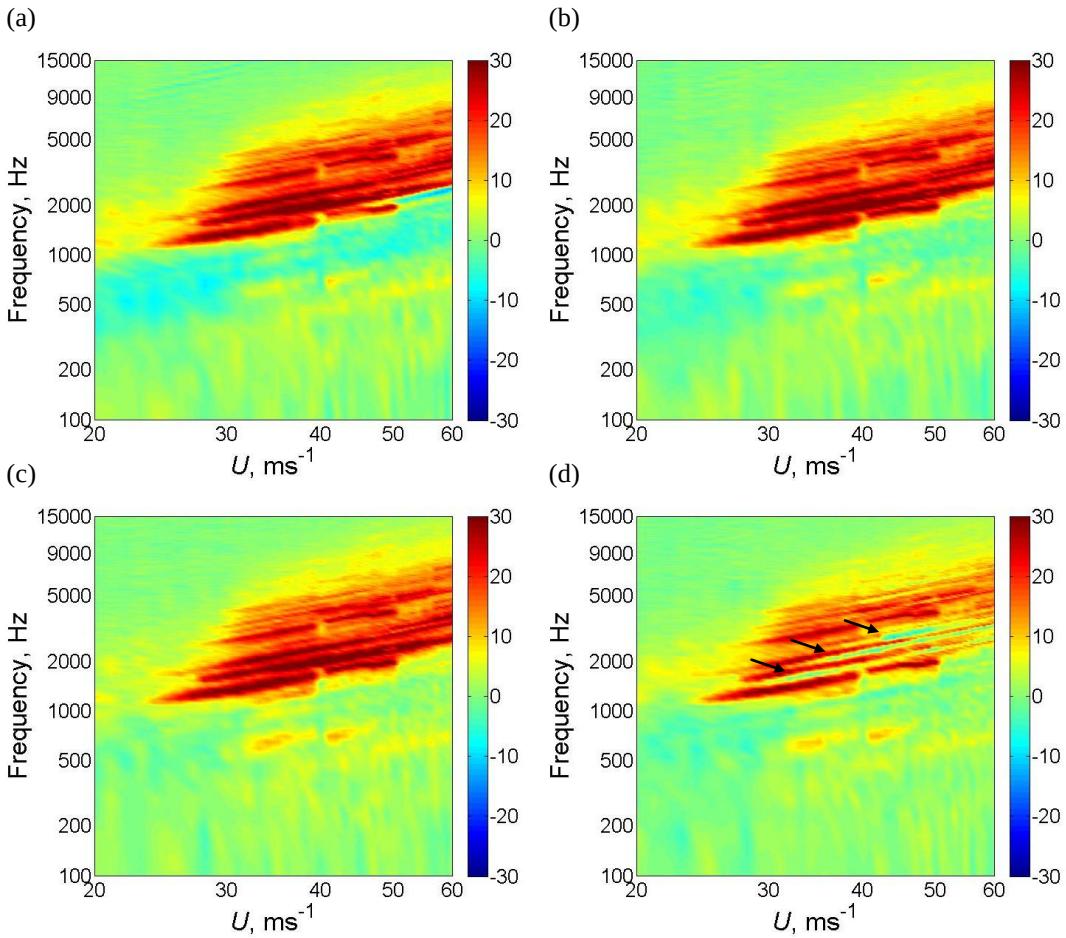

Fig. 10 Colormaps of the ΔPWL, decibel, for the instability tonal noise reduction by using a) S1, b) S2, c) S3, and d) S2* serrated trailing edges. The airfoil is set at θ = 4.2 deg.

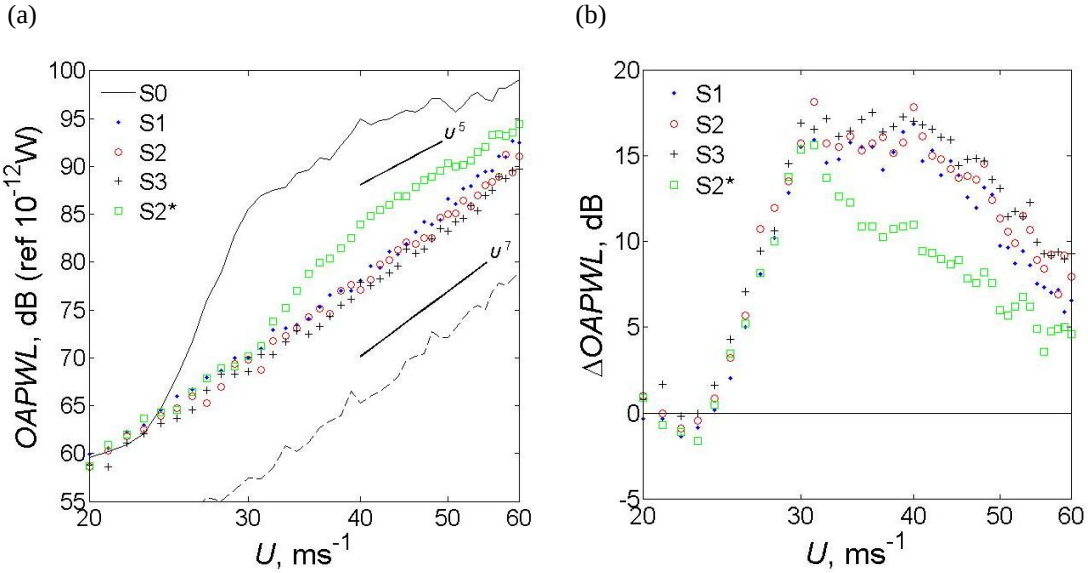

Fig. 11 Distributions of the untripped airfoil a) OAPWL with mean flow velocity at θ = 4.2 deg, including the background noise (- - -), and b) ΔOAPWL for the instability tonal noise reduction with mean flow velocity for the serrated trailing edges.

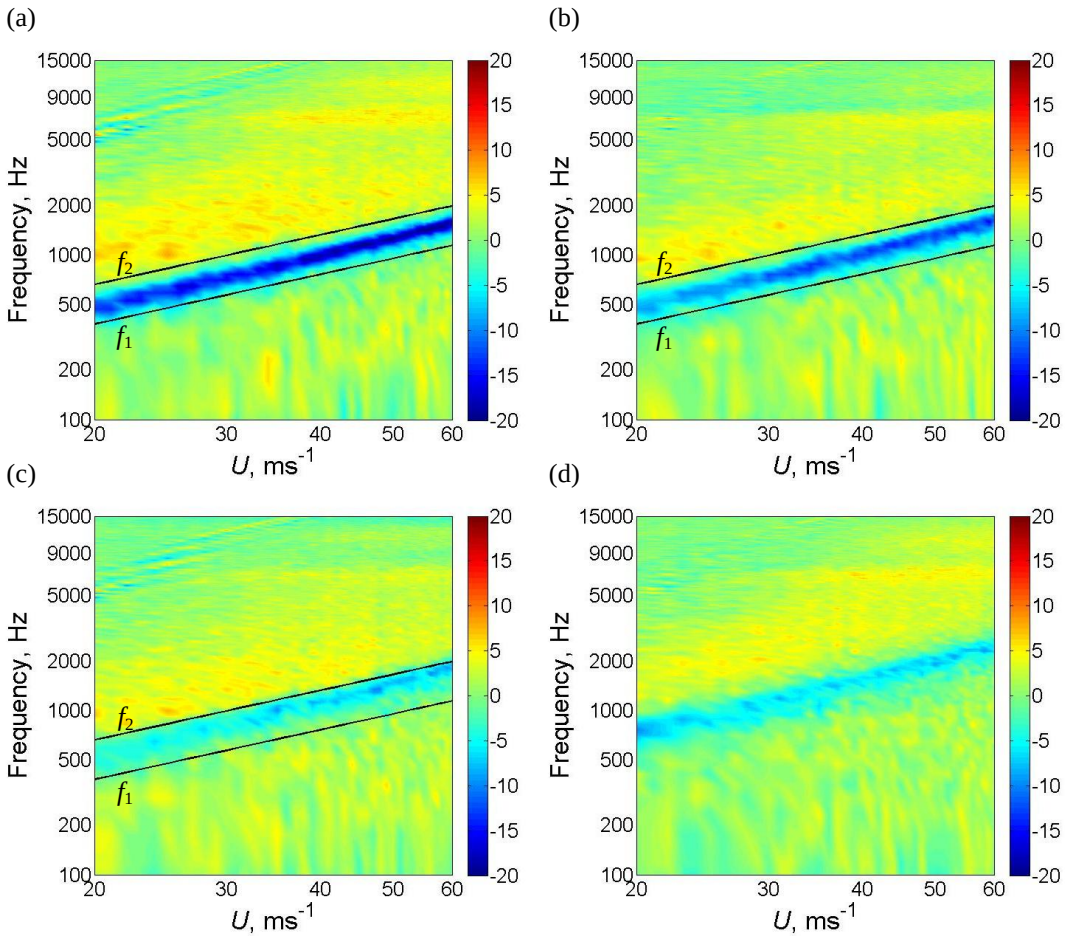

Fig. 12 Colormaps of the ΔPWL, decibel, for the broadband noise reduction by using a) S1, b) S2, c) S3, and d) S2* serrated trailing edges. The airfoil is set at θ = 4.2 deg.

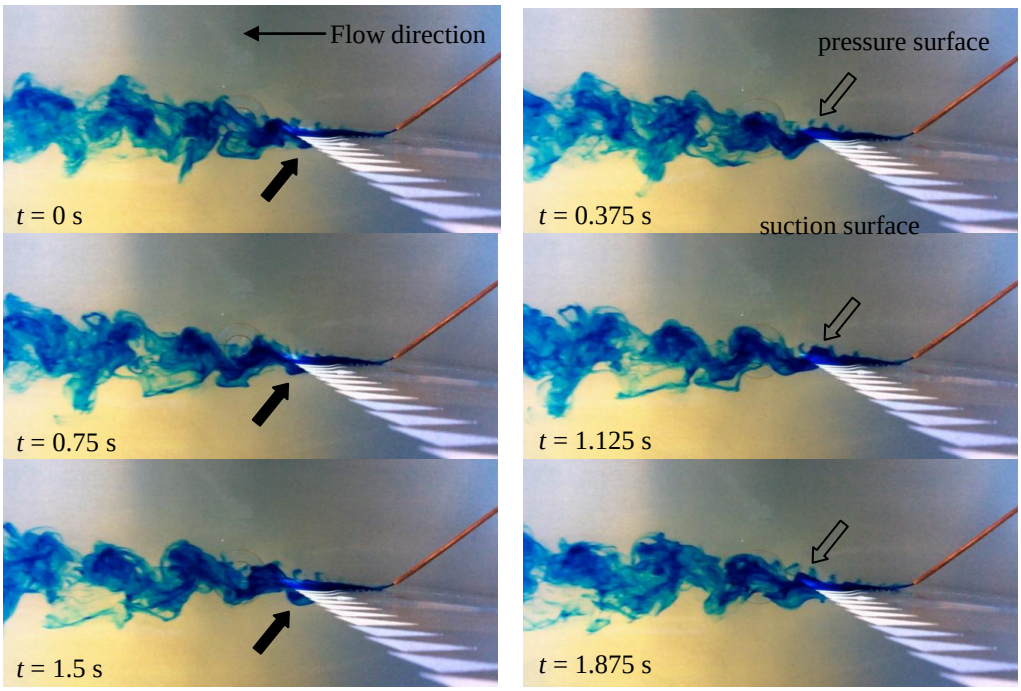

Fig. 13 Sequence of wake flows produced by a S3-type serrated trailing edge at $\theta = 5$ deg in a water tunnel.

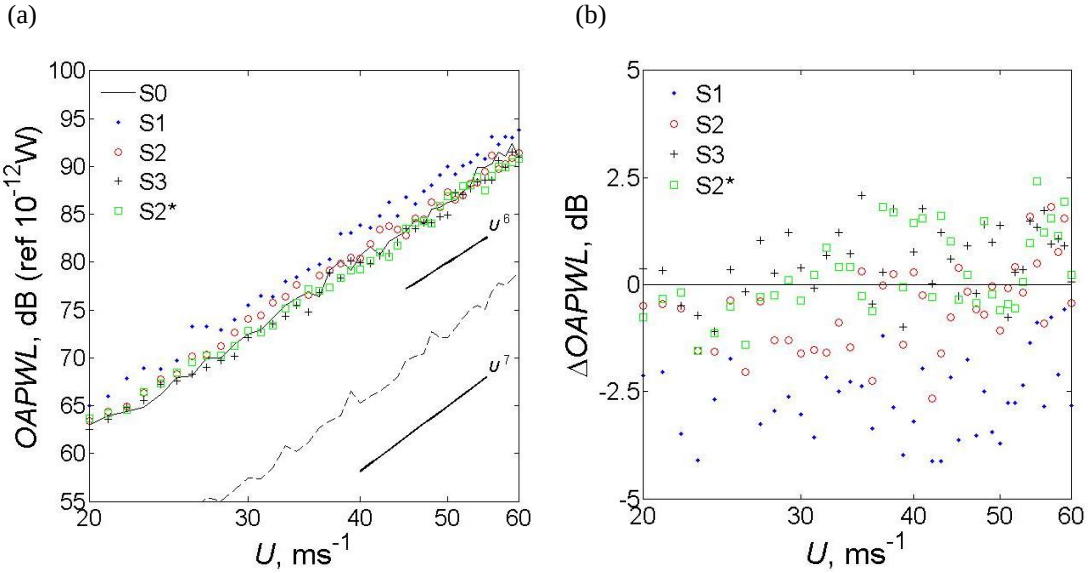

Fig. 14 Distributions of the tripped airfoil a) OAPWL with mean flow velocity at θ = 4.2 deg, including the background noise (- - -), and b) ΔOAPWL for the broadband noise reduction with mean flow velocity for the serrated trailing edges.

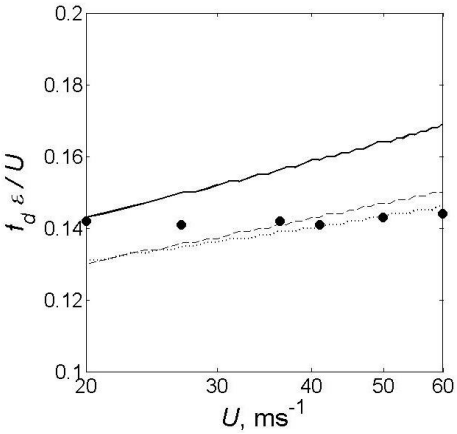

Fig. 15 Distributions of the Strouhal number of the vortex shedding noise produced by a tripped airfoil versus U for S1 (·····), S2 (- - -), S3 (—) and 2D-blunt (same ε, but with φ and λ/h = 0, represented by •) trailing edges at θ = 4.2 deg.

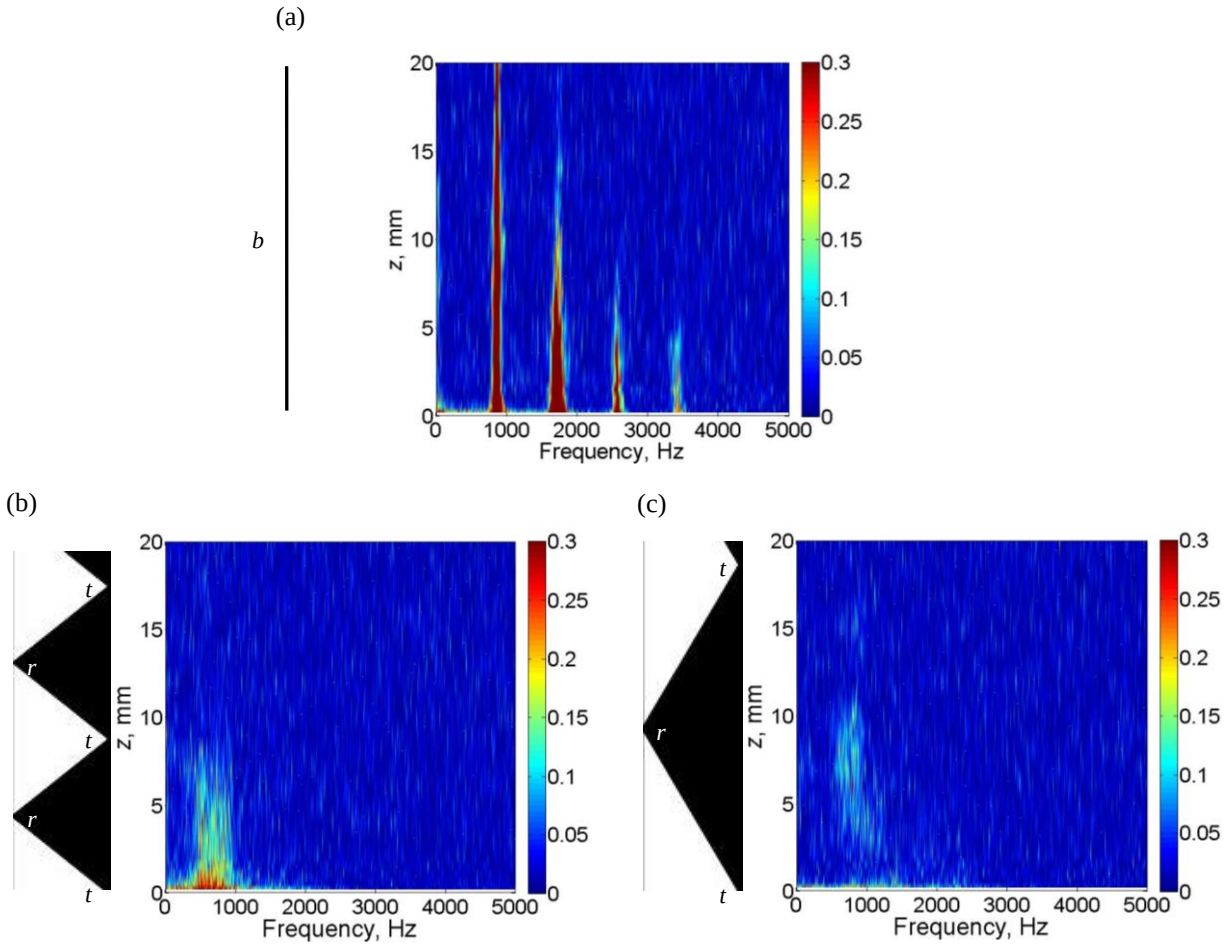

Fig. 16 Color maps of γ^2 for the a) SB, b) S2, and c) S3 trailing edges measured at θ = 5 deg and U = 20 ms^{-1}. '*b*', '*r*' and '*t*' denote 'blunt', 'root' and 'tip' respectively.

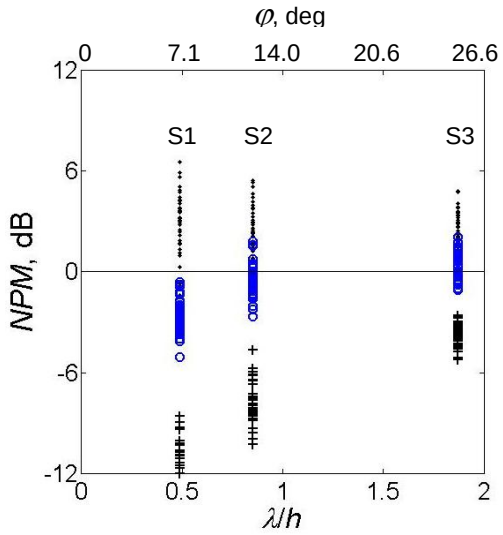

Fig. 17 Distributions of the NPM versus φ or λ/h for different frequency bands I (o), II (•) and III (+) at θ = 4.2 deg.